Dear RED

Project Completion report is attached
UC is being sent separately Tanmay;
(DRD/Chem.Sc/TKM/2095)

A Report on

Development of Bio Nanocomposite for Removal of Contaminants from Water

DRLT-P1-2011/TASK-45

(21.7.2011-20.1.2015)

Submitted by

Prof. T. K. Maji

& Dr. A. J. Thakur

Department of Chemical Sciences

Tezpur University, Napaam, Tezpur-784028

S. Mukherjee
Accn
06/10/16

INTRODUCTION

Problems associated with heavy metal, microbial and fluoride contaminations have drawn the interest of researchers since last decade. Researchers are engaged for developing methods to remove efficiently these hazardous materials from contaminated water. Some of the reported methods are chemical precipitation, membrane separation, ion exchange, electrochemical methods, adsorption etc. Among these, adsorption is considered as the most preferred method especially at low concentrations in recent times. It is associated with low cost, easy operation and trivial use of chemical additives. Also it has reusability.

In this regard, different materials like activated carbon, clay, metal oxides, various synthetic and natural polymers etc. have already been established as good adsorbing materials. Moringa oleifera seed extract, another naturally abundant material has potential in this field. Earlier studies have shown that Moringa Oleifera is non-toxic and can be used as a coagulant. Moringa Oleifera has an added advantage over the chemical treatment of water because it is ecofriendly as well as as edible. Clay is also reported to remove various heavy metals. Nano sized material like metal oxide has also drawn the attention of scientists recently for waste water treatment due to their high surface areas. But the separation of the nanomaterial after water treatment is quite expensive. Moreover, the question of their stability in diverse treatment conditions arises. Clay and other nanomaterials in combination with polymers have not been explored much for removal of various contaminants present in water. Most of the available reports addressed the use of Moringa as coagulant for removal of contamination. But hardly there is any report where it has been used for removal of arsenic, fluoride etc. from water.

These nanomaterials can be tailored by using polymers. Chitosan bio polymer represents an attractive alternative as adsorbents. It is largely available in nature, bio-compatible, non-toxic and bio-degradable as compared to the synthetic polymers. These excellent properties are attributed to the chemically reactive functional groups like hydroxyl, acetamido, amino groups etc. which makes chitosan an edge over others. Crosslinking of nanomaterial embedded in polymer is done to enhance its uses over a broad chemical environment. For metal removal applications, an adequate surface modification of the nanoparticles is a critical aspect regarding both selectivity and aqueous stability of these materials. These materials can play a vital role in improving the properties of composites based on biopolymers. The aim of this work is to develop a suitable biocomposite and study its efficacy for removal of contaminants mainly arsenic, fluoride etc.from contaminated water.

EXPERIMENTAL

Materials

Chitosan (medium molecular weight), Monmorillonite K-10 and Sodium arsenate heptahydrate ($AsNa_2O_4.7H_2O$) $FeCl_3.6H_2O$ and $FeCl_2.4H_2O$ were purchased from Sigma-Aldrich, USA. Glutaraldehyde solution (25%), Sodium fluoride (NaF) and NaOH was purchased from Merck, Mumbai, India. De-ionised water was obtained from Milli-Q water purification system (Millipores.A.S.67 120 MOLSHEIM, FRANCE). Dried *Moringa oleifera* (MO) seeds were obtained locally. All the reagents were of analytical grade and used without further purification.

I. Chitosan-Clay Nanocomposite

Preparation: Two types of nanoparticles were prepared for the adsorption test; one without nanoclay (NP) and other with the clay mineral (NPC). For the preparation of the nanoparticles, Ionic-Gelation technique was followed as suggested by Racovita with some modifications. 1g of chitosan polymer was dissolved in 200 mL 1% acetic acid solution under magnetic stirring. It was then transferred to a 500 mL round bottom (RB) flask and re-precipitated by adding 0.1M NaOH solution dropwise under high mechanical stirring. For NP type of adsorbent, as soon as precipitate formed, gluteraldehyde crooslinker was added to it and allowed to cross link at 45^0C. In the second case, clay solution dispersed in water was added to the acidic solution of chitosan, shaked vigorously with mechanical stirrer and sonicated (UP 200 S, Hielscher-Ultrasonics-GmBH, Germany). Now, precipitation was done by dropwise addition of NaOH solution under high stirring condition. This was followed by the drop wise addition of the gluteraldehyde crosslinker and allowed for cross linking under similar condition as mentioned in the former case. Varying amounts of crosslinker and nano clay were used to optimize the adsorption efficiency of the adsorbent nanoparticles and to enhance its stability in different experimental conditions. The reddish brown precipitate of nanoparticles was washed several times with double

distilled water to remove the excess NaOH left in the reaction mixture, dried and kept for subsequent use.

Results and Discussion

Characterization

FT-IR analysis

Fig. 1. represents the FTIR spectra for the clay (curve-a), chitosan polymer having high DDA(99%) (curve-b), NP(curve-c) and NPC (curve-d). FTIR spectrum of clay(curve a) shows the presence of bands at 3436 cm^{-1} for –OH stretching, 1625 cm^{-1} for –OH bending, 1052 cm^{-1}, 530 cm^{-1} for oxide band of metals (Al, Mg, Si, etc.). Chitosan polymer was characterized by the absorption bands (shown in curve- b) appeared at 3440 cm^{-1} (–OH stretching), 2965 cm^{-1}(–CH_2 stretching), 1617 (amide I band), 1410 (C-H bending), 1083 (C-N stretching corresponding to ammine). From the curve-c it was observed that the band at 3440 cm^{-1} (H bonded –OH stretching), present in the chitosan polymer showed a decrease in peak intensity in the NP.

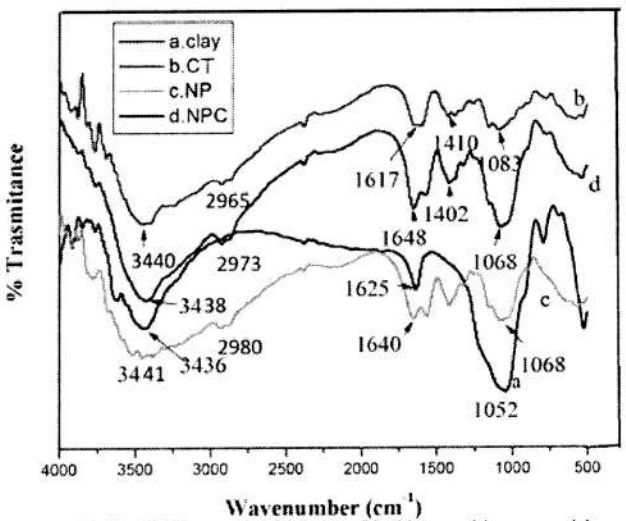

Fig.1. FTIR spectra of (a) clay, (b) chitosan (c) nanoparticle (d) clay loaded nanoparticle

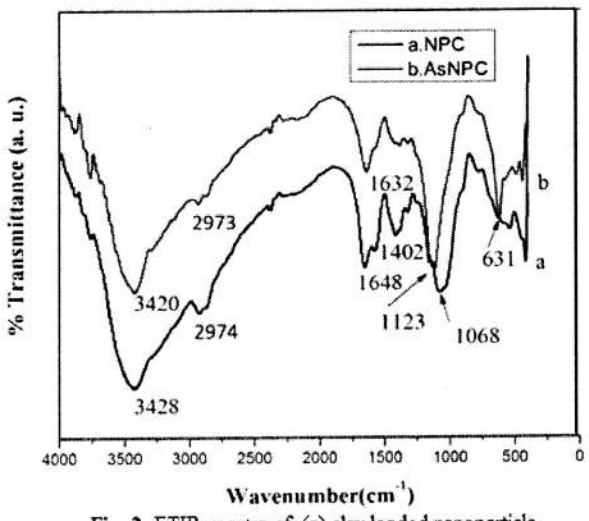

Fig. 2. FTIR spectra of. (a) clay loaded nanoparticle and (b) As (V) adsorbed nanoparticle

This indicated the structural changes that may occurred during the experimental conditions of their preparation. However, in NPC (curve-d) the peak intensities of –OH stretching and metal oxide bands were increased. The increase in peak intensity as mentioned above in NPC might be due to the incorporation of clay in to the system. Another important band near 2965cm^{-1} in the polymer, characteristic of -NH_3^+ overlap with –CH stretching (2967cm^{-1}) ,showed a red shift in both the cases and intensity of the NP remained almost same while that of NPC increased to some extent which may be due to the same reason as explained as above. The band near1410 cm^{-1} in the polymer shifted to lower wave number in the NP. The intensity of the band was also found to increase. The intensity further increased after incorporation of clay in to the system. Moreover the the peak intensity at 1068 cm^{-1} enhanced compared to that of NP suggesting the interaction of the clay with the polymer.

In Fig. 2. clay loaded nanoparticle and As adsorbed NPC are shown. From the figure it was observed that the bands at 3428 cm^{-1}, 1648 cm^{-1}, 1068 cm^{-1} of the NPC became sharp after the treatment with As (V) solution. Along with an increase in intensity, the band at 1068 cm^{-1} also showed a red shift to 1123 cm^{-1} when treated with As (V) solution. All these changes in FTIR band indicated the interaction of the metal ion with the nanocomposite.

X-Ray Diffractometer analysis

The XRD patterns of clay, chitosan polymer, polymer nanoparticles (without clay) and clay loaded nanoparticles are shown in Fig. 3.

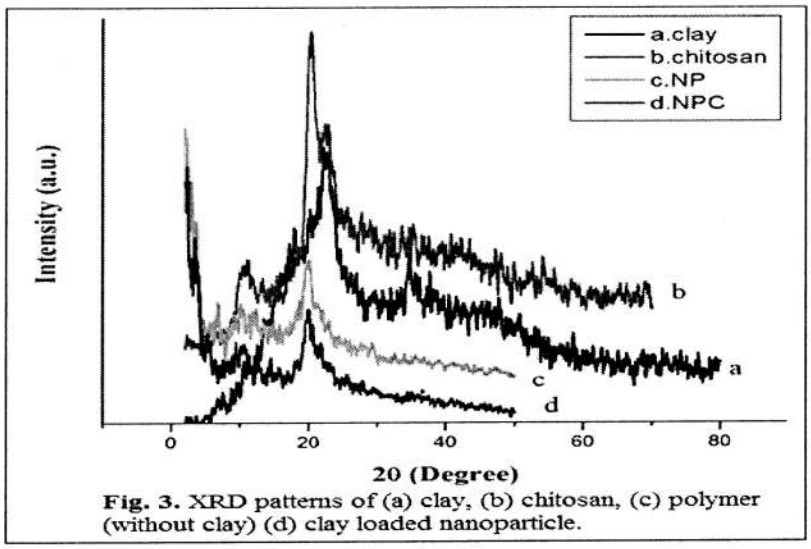

Fig. 3. XRD patterns of (a) clay, (b) chitosan, (c) polymer (without clay) (d) clay loaded nanoparticle.

From the figure, it was seen that the XRD pattern of the MMT clay shows a peak at $2\Theta=7^0$ and 22^0 corresponding to basal spacing's of 1.2 and 4.03 nm respectively (curve-a). The XRD pattern of chitosan showed the characteristic peak at $2\Theta = 10^0$, 20^0 and 25^0, respectively which corresponds to the literature data (curve-b). XRD pattern of the NP with CS (curve-c) shows that the intensities of the peaks at $2\Theta = 10^0$, 20^0 significantly reduced and the peak at 22^0 disappeared completely. This might be an indication of structural changes (change in crystalinity) occurred during the conversion of CS into chitosan NP. Chitosan has a large number of hydroxyl functional groups and also its cationic structure in acidic medium has a good miscibility with Na^+MMT. Hence it could easily intercalate into the silicate layers by cationic exchange.

On the other hand, in NPC (curve-d), the characteristic peaks for chitosan polymer at $2\Theta = 10^\circ$ and 20° with decreased intensity was observed. Moreover, the shifting of crystal diffraction peak of clay to lower angle of 2θ (mention the value) value was observed. The reduced peak intensities as compared to the pristine polymer indicated the diminish crystallinity in the NPC. This suggested a molecular level dispersion of clay layers in the polymer matrix.

Scanning Electron Microscopy(SEM) study

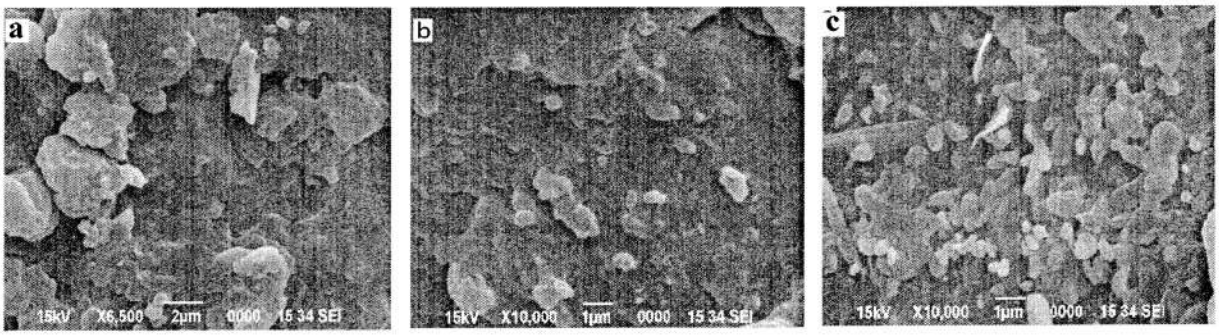

Fig. 4. SEM images of (a), (b) NPC, (c) As(V) adsorbed NPC.

SEM images of the clay loaded nanocomposite before and after As (V) adsorption are shown in Fig. 4. The change in the surface morphology of the nanocomposites before and after As (V) treatment indicated the structural changes occurred in the nanocomposite due to adsorption of As(V).

Transmission Electron Microscopy (TEM) Study

Fig. 5. showed the TEM images of chitosan polymer(fig. 5. a), clay loaded nanocomposite (fig. 5.b and fig. 5.c). In the micrograph good exfoliation of clay layer within the polymer matrixwas observed.

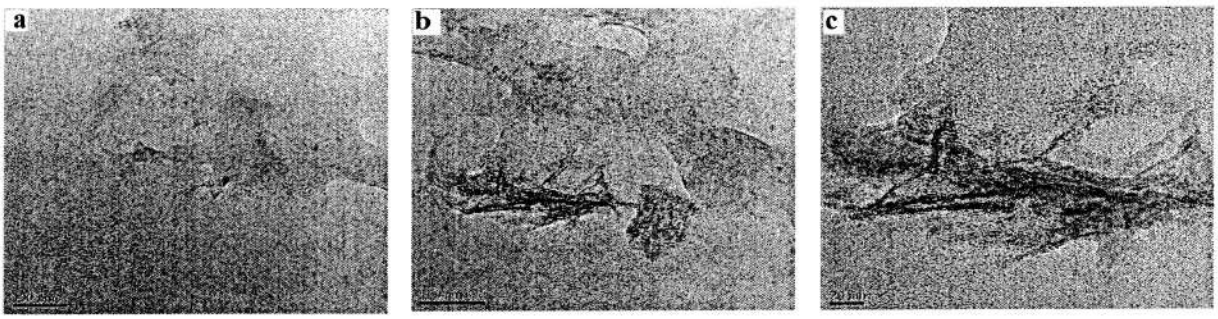

Fig. 5. TEM micrographs of (a) chitosan polymer and (b), (c) clay loaded nanocomposite

Batch adsorption experiment for As(V)

Effect of Nanocomposite Dose

Fig. 6. Showed the effect of dose of nanoparticles on % removal of As(V).The adsorption study were carried out with different doses ranging from 0.1 to 3 g/L of the nanoparticle with 500 µg/L of initial As(V) concentration. It was found that a dose of 0.5g/250 mL of solution was sufficient for maximum removal of As(V).

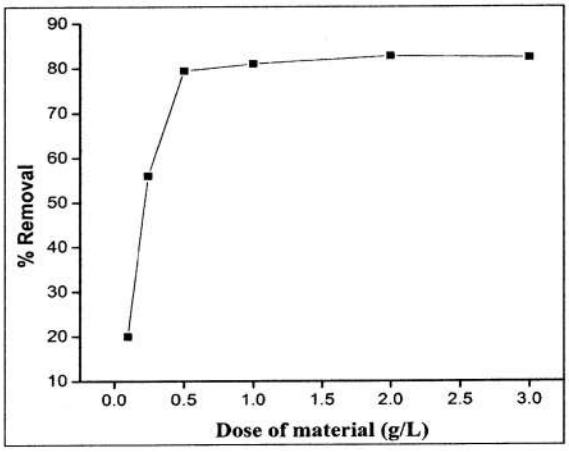

Fig. 6. Effect of dose of material

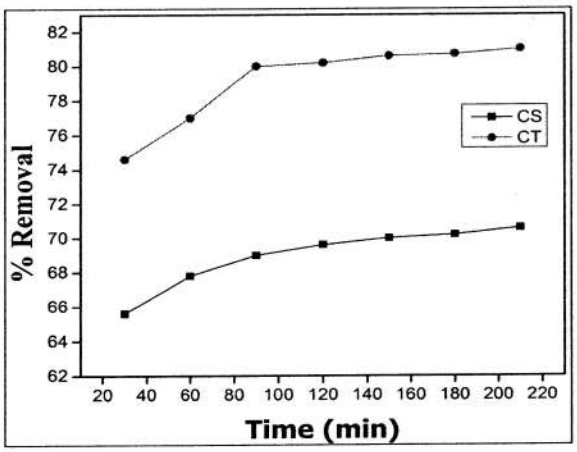

Fig. 7. Effect of agitation time

Effect of clay on As(V) removal

Fig.7. Shows the variation of As(V) adsorption with time for both clay incorporated nanoparticles and nanoparticle without clay. To study the effect of time and clay content the concentration of As(V) solution was kept at 500 µg/L and material dose of was fixed at 2 g/L as optimized earlier. From the plot it was observed that due to the loading of clay significant improvement in As(V) adsorption was obtained. This improvement in efficiency of adsorption may be due to the high sorption, ability to expand and ion exchange property of the clay mineral.

Effect of pH on As (V) removal

The batch tests were carried out under different pH conditions (Fig. 8). It was found that the optimum condition for adsorption was at pH $\leq$ 3.0. This is attributed to the existence of arsenate ions in different oxidation states viz. H_3AsO_4, $H_2AsO_4^-$, $HAsO_4^{2-}$ and AsO_4^{3-} at different pH conditions 2.0, 2.0-7.0, 7.0-12.0, and ›12.0 respectively. Another reason for more binding of

arsenate at low pH is due to the protonation of the amine groups which makes it positively charged and hence anion binding capacity increases.

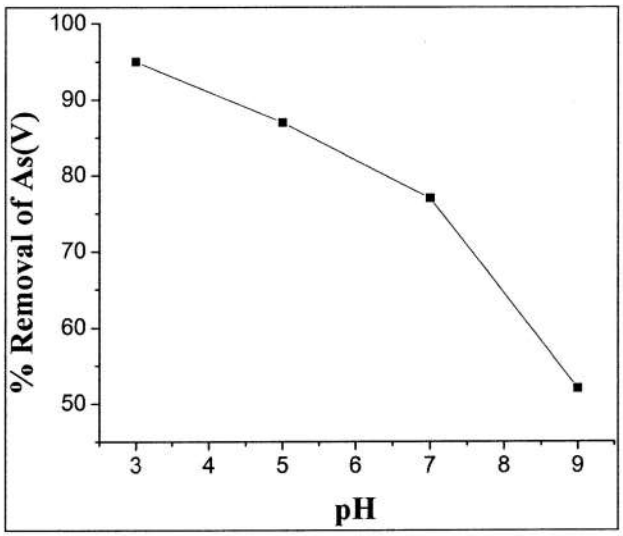

Fig. 8. Effect of pH on percent removal of As(V)

II. Chitosan-MO(CSMO) and Chitosan-MO-clay composite Systems

Preparation

A CSMO composite system was prepared by Ionic-Gelation technique as suggested by Racovita with some modifications. Initially 1g of chitosan biopolymer was dissolved in 200 ml 1% acetic acid solution under stirring condition. At the same time equal amount of MO seed powder was dispersed in small amount of distilled water for several hours. The seed powder dispersion was then poured slowly to the polymer solution under stirring condition so that a stable dispersion was formed. After well mixing of the two components, chitosan was reprecipitated by adding NaOH (0.1 M) solution to the mixture. It was then cross linked with Gluteraldehyde solution (23 %) which was further diluted before use. The temperature was maintained at 40 ^{0}C and the crosslinking reaction was allowed to take place for several hours. Then it was filtered, dried and finally grinded to powder for further use.

A CSMO-clay composite system was also developed following the same method as described above. The clay (5% w/w) was dispersed in distilled water using mechanical stirrer for 24 h. It was followed by sonication (UP 200 S, Hielscher-Ultrasonics-GmBH, Germany). Then it was

added to the CS-MO dispersion, precipitated, crosslinked, dried and made ready for further use. A chitosan clay composite system was also produced for comparison purpose.

Results and Discussion

Characterization

Fourier Transformed infrared spectra (FTIR)

Fig.9. shows the FTIR spectra of the prepared CSMO and the MO seed powder.The characteristic band for MO at 3272-3469 cm^{-1}(O-H or N-H stretching), 2924 cm^{-1} (C-H stretching), 1744, 1657 cm^{-1} (C=O stretching), and 1236 cm^{-1} (C-N stretching) appeared in the CSMO composite indicated the incorporation of MO in the composite. Also the intensity of the band in the region 3272-3469 cm^{-1}(O-H or N-H) decreased in the CSMO system. The peak in chitosan appeared at 1410 cm^{-1} due to O-H bending was found to shift at 1454 cm^{-1} and another peak at 1083 cm^{-1} disappeared completely in the CSMO composite. These change in band intensities or band positions in the CSMO as compared to the MO or chitosan polymer indicates structural changes in the combined system and some new probable interactions in the combined system.

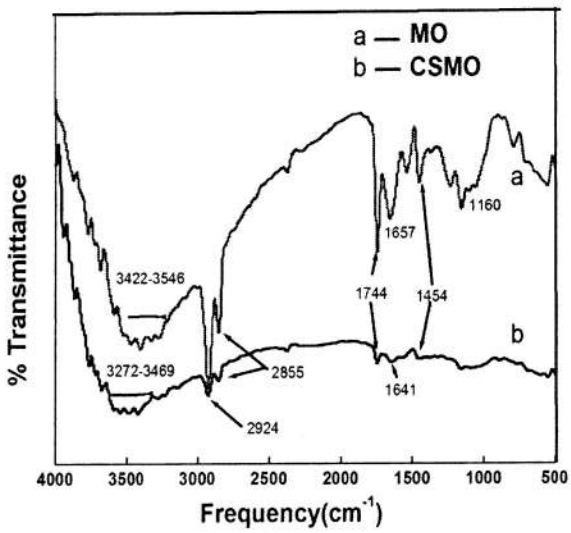

Fig.9. FTIR spectra for MO and CSMO systems

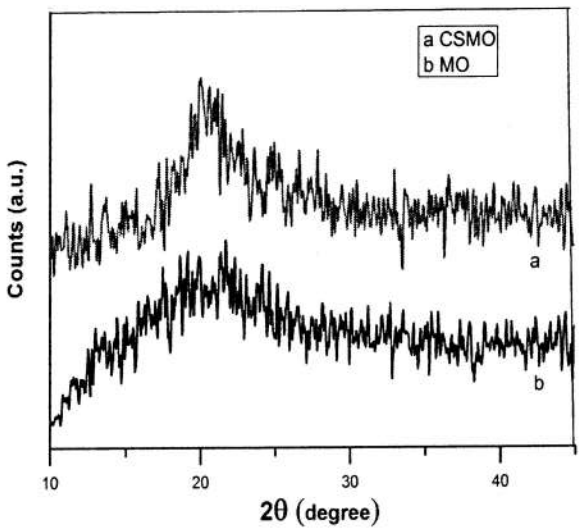

Fig.10. XRD pattern of the MO and CSMO

X-Ray diffraction (XRD) analysis

In the XRD pattern (Fig. 10) of the MO seed broad peak was observed indicating its amorphous nature. But in the combined system a prominent peak at $2\theta=22^0$ is observed which corresponds to the $2\theta=22^0$ peak in chitosan with diminished intensity. Also the peak at $2\theta=20^0$ in chitosan (Fig. 3) disappeared in the combined system. These changes in XRD pattern of the combined system as compared to original materials indicated good dispersion of MO in the composite.

Batch Adsorption Test for Fluoride (F^-)

Effect of dose of MO seed powder on fluoride removal

Batch studies were conducted in a temperature-controlled shaker (water bath incubator shaker, NSW, INDIA, CE0434) using F^- concentration of 5mg/L (initial) and varying the adsorbent dosage in the range 4g/L to16g/L. The agitation speed of the shaker was fixed for all batch experiments.

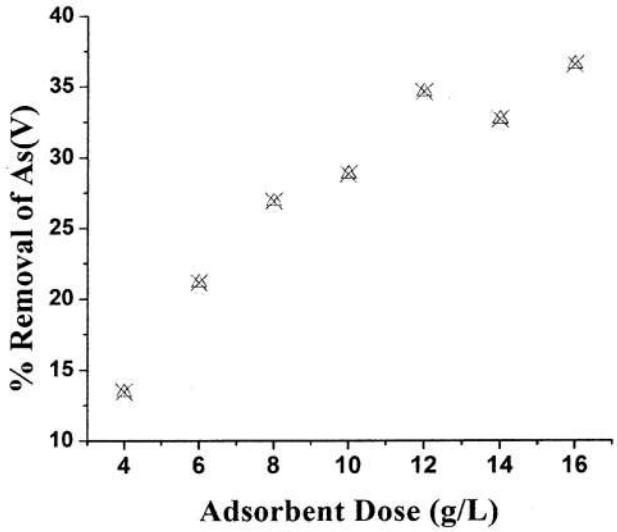

Fig. 11. Optimisation of MO seed dose for maximum removal of fluoride

Effect of pH on Fluoride Removal

It was found that the removal of fluoride by MO seed powder was affected by pH, and alkaline pH (~9) was found to be favorable for this purpose. Again in acidic pH (~3), the removal was better than that in neutral condition. Better result in alkaline condition (Table. 1) may be due to

increase of hydroxyl ion concentration in the solution. Hence the rate of fluoride ion sorption was maximum on the active surface, due to cation ion exchange phenomenon of alkali treated *Moringa oleifera* bioadsorbents at high pH value. Again, in acidic pH the large number of ammine functionality present in the amino acid chains of MO seed becomes NH_3^+ which now can combine with fluoride readily by electrostatic attraction.

Table. 1. Defluoridation by MO seed powder at different pH

Material	pH (~)	Initial fluoride concentration (mg/L)	Fluoride left (mg/L)
MO seed	3	5.2	3.9
	7	5.2	4.2
	9	5.2	3.7

Effect of Time on percent removal of fluoride ion

Batch studies were conducted for different time intervals keeping the dose of MO seed powder fixed at 12 g/L. It was found that the optimum time for maximum removal of fluoride with an initial fluoride concentration of 6 mg/L is 90 minute.

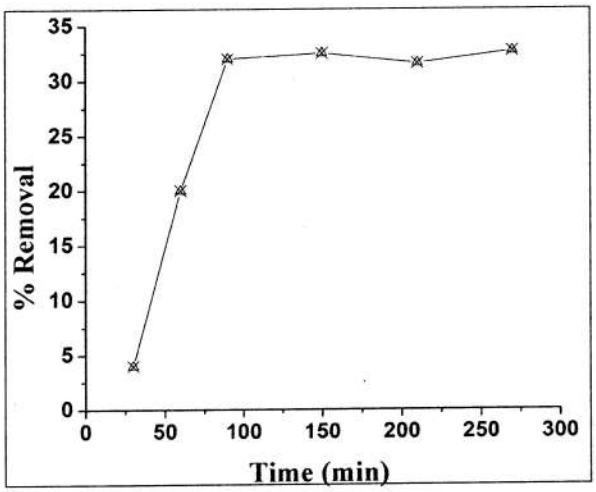

Fig. 12. Effect of time on percent removal of fluoride by MO seed powder

Comparison of CSMO with MO

Keeping the material dose fixed at 12 g/L and pH of the treated water at 9, batch test were carried out with MO seed powder, chitosan and CSMO. Initial concentration of the fluoride contaminated water was kept at 5.6 mg/L. Table.2. shows the efficacy of the combined CSMO system as compared with the original MO seed powder and chitosan biopolymer. It was observed that the efficacy of CSMO composite was higher than chitosan but almost similar to that of MO seed powder

Table.2. Comparison of efficiency of combined system with MO seed and chitosan polymer

Material	Amount g/L	Initial F^- concentration (mg/L)	% removal of fluoride
MO			28.57
Chitosan	12	5.6	19.64
CSMO(1:1)			26.78

.

III. Chitosan Coated Magnetite Nanoparticle System

Preparation

Fe_3O_4 nanoparticles were prepared in two steps by an ex-situ method. Initially Fe_3O_4 nanoparticles were synthesized by co-precipitating Fe^{2+} and Fe^{3+} (2:3 w/w) ions followed by treating under hydrothermal condition. A 1% (w/v) chitosan solution was prepared simultaneously by dissolving requisite amount of chitosan biopolymer in 1% (v/v) acetic acid solution. To this chitosan solution magnetite nanoparticle in suspension form was poured and mixed for several hour under high stirring. Chitosan was precipitated using the NaOH solution. The temperature of the reaction vessel was brought down to below room temperature. Then Gluteraldehyde solution was added dropwise to the mixture under high stirring condition. The temperature was then raised gradually to 50° C and the reaction was continued for 2 h under continuous stirring. The temperature was then brought down to room temperature. The nanoparticle thus formed was filtered, washed with de-ionized water, dried and kept ready for subsequent applications.

Results and discussion

Characterization

FT-IR analysis

Fig.13. shows the FT-IR spectra of (a) chitosan polymer (CT), (b) bare Fe_3O_4 nanoparticles (FeN) and (c) chitosan coated Fe_3O_4 (CTN) nanoparticles.

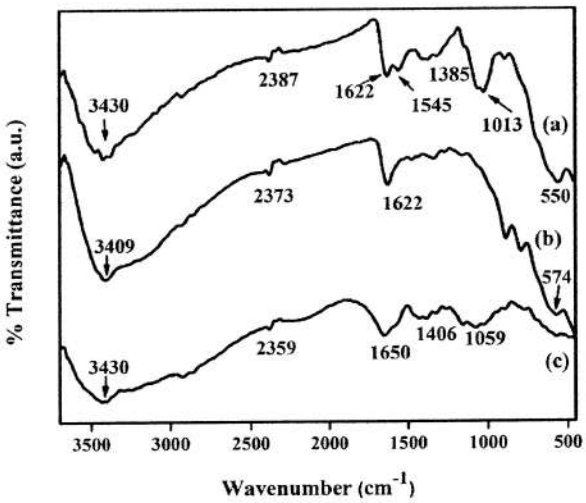

Fig. 13. FT-IR spectra of (a) CTN, (b) FeN

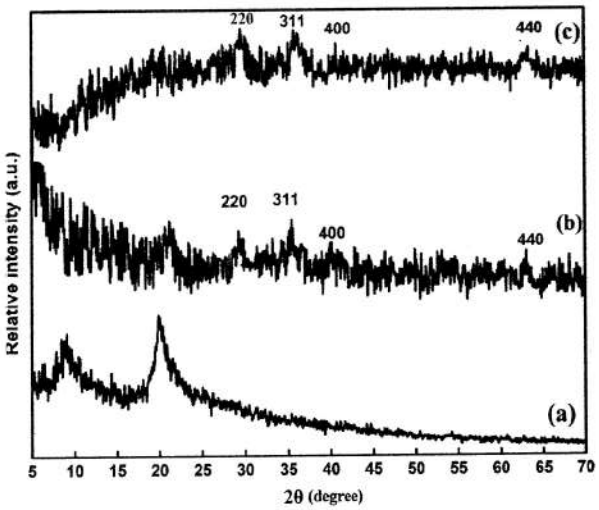

Fig. 14. XRD spectra of (a) CT, (b) FeN and (c) CTN

Chitosan polymer was characterized by the absorption bands appearing near 3350-3450 cm^{-1} (-NH stretching), 2359 cm^{-1}(–CH_2 stretching), 1650 cm^{-1}(amide I band), 1406 cm^{-1} (C-H bending), 1059 cm^{-1} (C-N stretching corresponding to amine). In the spectrum for FeN, three characteristics bands appeared at 574, 1622 and 3409 cm^{-1}. The band at 574 cm^{-1} resembles the vibration of the Fe-O bonds in the crystalline lattice of Fe_3O_4 as reported earlier. Bands at 1622 and 3409 cm^{-1} might be due to the hydroxyl groups which were accumulated on the surface of the nanoparticles during the preparation of FeN by the chemical co-precipitation method. In CTN, the presence of Fe_3O_4 core could be identified by the strong stretching absorption band at 550 cm^{-1}, which corresponded to the Fe–O bond. The absorption band appered in the 550 cm^{-1} region was in chitosan-coated nanoparticles spectrum, suggested the formation of magnetite nanopartciles. The presence of band around 1545 cm^{-1}, assigned to the -NH_2 group bend scissoring, in chitosan-coated nanoparticle's spectra, suggested the successful coating of magnetite nanoparticles by chitosan polymer.

X-Ray Diffraction (XRD) study

The crystal structures of chitosan, bare Fe_3O_4 nanoparticles and chitosan coated Fe_3O_4 nanoparticles were studied using XRD(Fig. 14.) The XRD spectrum of chitosan shows peaks with low intensity values around $2\theta = 9°$ and a broad peak at around $2\theta = 20°$. Similar results were reported by Li et al. and Lu et al. Diffraction peaks appeared at 2θ of 36°, 42°and 63.5° due their corresponding indices (311), (400) and (440) were observed in FeN nanoparticles. These were the characteristic peaks of the magnetite (Fe_3O_4) crystal having an inverse cubic spinel structure.

In the diffractogram of chitosan coated FeN nanoparticles,the peak positions assigned for Fe_3O_4 crystals remained unchanged. This suggested that the chitosan binding process did not result in the phase change of Fe_3O_4.

Thermogravimetric analysis

All the three samples exhibit their own distinctive TGA curves(Fig. 15). The initial weight loss observed in all the samples at around 100 °C was due to the evaporation of the small amount of moisture present in the samples. The TGA curve for Chitosan showed the highest weight loss in the temperature range ~250 °C - 320 °C; whereas the bare Fe_3O_4 nanoparticles (FeN) had hardly shown any weight loss in that region, except the initial loss of water. Chitosan coated Fe_3O_4 showed less weight loss compared to bare chitosan. It may be due to the increasing stability of chitosan achieved through interaction with FeN. Moreover, since no two separate degradation patterns were observed for the TGA curve of chitosan coated FeN nanoparticles (CTN), it indicated that the mixing of chitosan and FeN did not form a blend. Rather, chitosan properly interacted with FeN nanoparticles. There is not any significant weight loss for FeN nanoparticles from 100 °C to 500 °C. For the CTN, the weight loss from 220–400 °C was mainly due to degradation of cross-linked chitosan component present in the CTN nanoparticle.

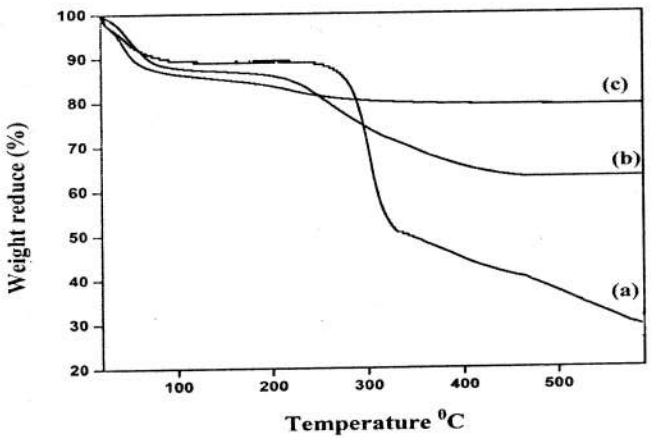

Fig. 15. TGA graphs of (a) CT, (b) CTN and (c) FeN

SEM and Energy Dispersive X-Ray(EDX) Analysis

Fig.16. shows the SEM images of chitosan, bare magnetite and chitosan coated magnetite nanoparticle. From the SEM micrographs it was observed that the chitosan nanoparticles are found to be agglomerated (Fig.16.a). The agglomeration of bare magnetite was less compared to chitosan nanoparticles(Fig.16.b). The agglomeration was least and the surface of the nanoparticles was smooth in CTN nanoparticles. Chitosan formed a coating over iron oxide nanoparticles and protected them from agglomeration.

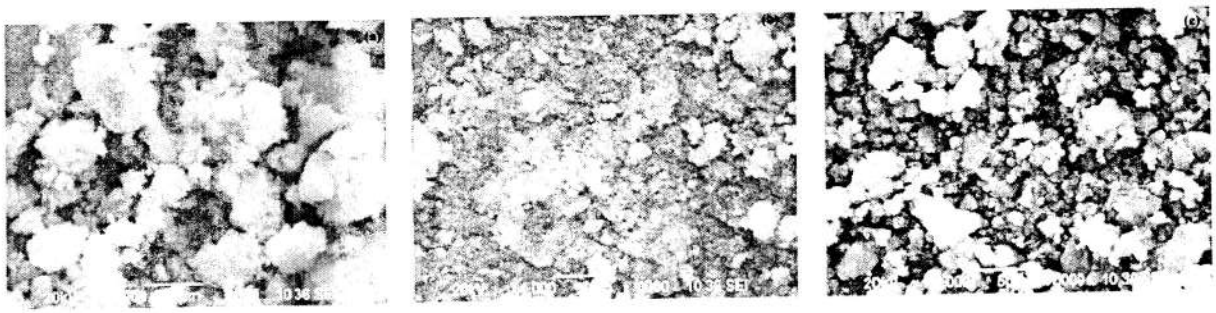

Fig. 16. SEM micrographs of (a) chitosan,(b) bare magnetite, (c) chitosan coated nanoparticle (CTN)

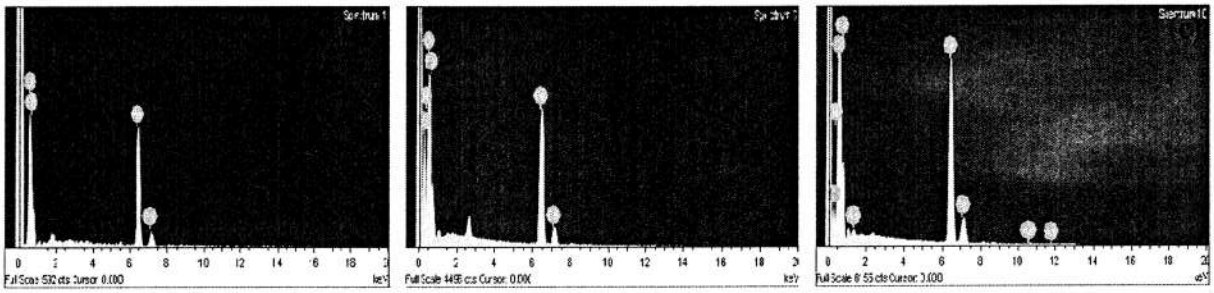

Fig. 17. Relative elemental compositions of (a) FeN, (b) CTN before adsoption and

(c) CTN after adsorption.

Fig.17. shows the relative compositions of different components of FeN, CTN before and after arsenic adsorption. The EDX data showed the distribution of different components in the composite individually and as a whole. It was confirmed that As(V) is well adsorbed on the surface of CTN particles (fig.17.c).

Batch Adsorption Experiment for As(V)

Effect of adsorbent dose for percent removal of As(V)

The effect of adsorbent dose at a fixed As(V) solution concentration (0.6 mg/L) and near neutral pH on percent removal of As(V) is shown in Fig.18. It was observed that the removal efficiency increased up to certain adsorbent dose beyond that the efficiency remained almost constant. The concentration of adsorbent was varied from .01 to 0.4 g/100mL. At low adsorbent dose the available active sites were not sufficient to adsorb the required As(V) from its solution. With the increase in adsorbent dose the availability of more active sites facilitated the percent removal efficiency. It was observed that for a solution of 0.6 mg/L, a dose of 0.1 g/100mL was sufficient to adsorb efficiently. However at higher adsorbent dose no significant increase in percent removal was observed which is due to the attainment of equilibrium between the active sites and As(V) ions in solution.

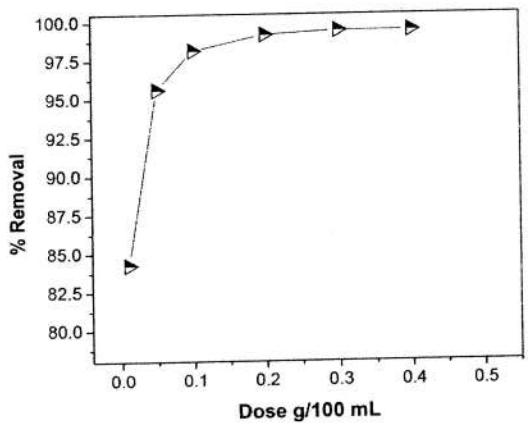

Fig. 18. Effect of adsorbent dose on As(V) removal

Influence of agitation time on percent removal of As(V)

Fig.19. shows the effect of agitation time on percent removal of the As(V) ion. The concentration of the As(V) solution and the amount of chitosan coated nanoparticles i.e. adsorbent (previously optimized) were kept fixed at 0.6 mg/L and 1g/L respectively and the experiment was carried out near neutral pH. Percent removal of As(V) was found to increase initially with the increase in contact time up to 120 min beyond that it remained unchanged. This might be due to the establishment of equilibrium between the active sites on CTN surface and arsenate ions from the aqueous phase. Studies shoed that CTN nanoparticles showed better removal capacity than bare iron nanoparticle (not shown in fig). This suggested the formation of more sorption sites caused by the increase in surface area of resultant nanoparticles due to stabilization by chitosan. Zhang et. al used starch stabilized nanoscale magnetite particles towards the remediation of arsenate contaminated soils and reported an improvement in adsorption affinity of nanoparticles towards arsenic. An et. al also reported that starch coated magnetite nanoparticles removed arsenic more efficiently than bare magnetite nanoparticles from spent ion exchanged brine.

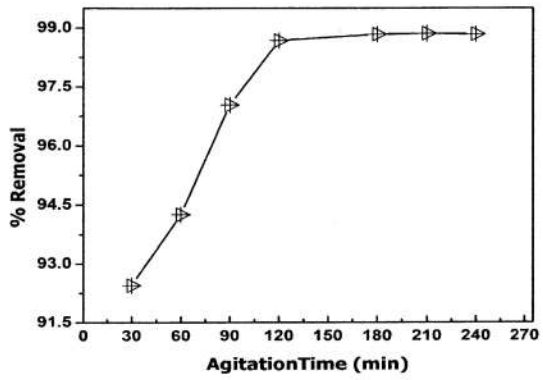

Fig. 19. Effect of agitation time on % removal of As(V).

Effect of initial As(V) concentration on percent removal

The effect of initial ion concentration on % removal of As(V) was studied in the concentration range of 0.4-4 mg/L. The agitation time and material dose was fixed as optimized earlier. Fig.20. shows the variation of percent removal of As(V) with change in initial As(V) concentration. It was observed that the percent removal of As(V) decreased with the increase in initial metal ion concentration. But the amount of metal ion uptake per unit weight of adsorbent (mg/g) increased. This might be attributed to the delayed establishment of equilibrium between the adsorbent sites and the As(V) ions due to increase in initial As(V) concentrations.

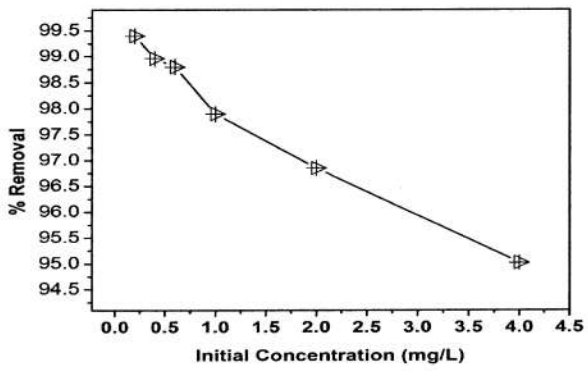

Fig. 20. Effect of initial As(V) concentration on % removal of the ion.

Adsorption kinetics

The kinetic study for the adsorption of As(V) was conducted at neutral pH. In order to investigate the sorption mechanism for removal process, pseudo first and second-order kinetic

models were used at different experimental conditions. The adsorption of As(V) was carried out for 2 h with intial As(V) concentration in the range 0.2-4 mg/L. The adsorption rate constants (K_{ad}) were calculated from Fig.21. using Lagergren's equation. A simple pseudo first order kinetic model, is represented as

$$\log_{10}(q_e - q_t) = \log_{10} q_e - \frac{k_{ad}}{2.303t} \qquad (1)$$

where, q_t is the amount of As(V) adsorbed in mg/g at time t, q_e is the amount of As(V) adsorbed (mg/g) at equilibrium and K_{ad} is the rate constant of adsorption (min^{-1}). Linear plots of log (q_e-qt) vs t (Fig.21.) show the applicability of Equation (1) for the material.

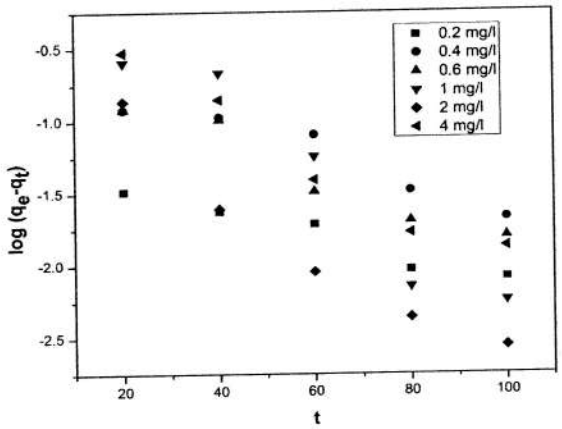

Fig. 21. Lagergren plot for sorption of As(V) on CTN

The k_{ad} values for different initial As(V) concentrations were calculated from slopes, the q_e values from the intercept of the respective linear plots. The correlation coefficients (R^2) were computed and the values are shown in Table.3.

Table. 3. Lagergren's constants for sorption of As(V) on CTN

*C_o (mg/L)	**Mass (g)	K_{ad} (min^{-1})	R^2
0.2	1.0	0.0186	0.935
0.4	1.0	0.0233	0.896
0.6	1.0	0.0286	0.913

1.0	1.0	0.0551	0.896
2.0	1.0	0.0476	0.919
4.0	1.0	0.0417	0.946

* C_o: Initial concentration of As(V) solution

** Mass of CTN (adsorbent) nanoparticles

In addition, pseudo-second-order model is also widely used. The simplest and the most popular linear form pseudo-second-order kinetic models is represented by the following equation

$$\frac{t}{q_t} = \frac{1}{h} + \frac{t}{q_e} \qquad (2)$$

Where, $q_t = q_e^2 kt/(1+q_t kt)$, the amount (mg/g) of As(V) adsorbed on the surface of material at any time t, k being pseudo-second order rate constant ($gmg^{-1}min^{-1}$), q_e is the amount adsorbed at equilibrium, and $h = kq_e^2$ (mgg^{-1} min^{-1}) is the initial sorption rate. The values of q_e, k and h can be obtained from the slope and intercept values of the curves of t/q_t vs t as shown in Fig.22. The correlation coefficients (R^2) were computed and all the values are shown in table.4.

Table. 4. Values of different 2nd order kinetic parameters at different initial As(V) concentrations

C_0 (mg/l)	Mass (g)	q_e	K	h	R^2
0.2	1.0	0.198	0.992	0.0392	0.998
0.4	1.0	0.398	0.162	0.0259	0.932
0.6	1.0	0.582	0.216	0.0733	0.962
1.0	1.0	1.114	0.069	0.0861	0.988
2.0	1.0	2.008	0.368	1.480	0.999
4.0	1.0	4.0367	0.125	2.030	0.999

The q_e values were found to increase with the increase in the initial As(V) concentrations. The curve for pseudo second order kinetics exhibited higher correlation co-efficient compared to pseudo first order model.

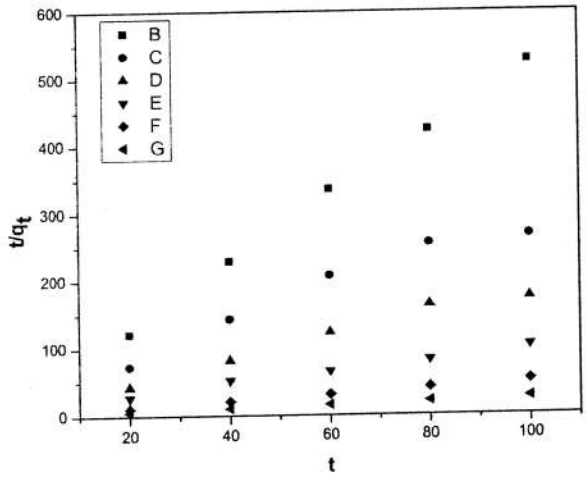

Fig. 22. Second order model for sorption of As(V) on CTN

Adsorption Isotherm

Both Freundlich and Langmuir isotherms were applied for the study of equilibrium adsorption of As(V) on chitosan coated Fe_3O_4 composite. The Langmuir isotherm is represented by the following equation

$$\frac{C_e}{Q_e} = \frac{1}{Q_0 b} + \frac{C_e}{Q_0} \qquad (3)$$

Here *Ce* is the equilibrium concentration (mg/L), Q_e is the amount of As(V) adsorbed at equilibrium (mg/g), and Q_0 and b are Langmuir constants related to the adsorption capacity and energy of adsorption, respectively.

The linear plots of C_e/Q_e vs.*Ce* show that adsorption follows the Langmuir isotherm model (Fig. 23). The correlation coefficient was 0.947. Q_0 and b were determined from the slope and intercept of the plot and were found to 1.48 mg/g and 123.75 L/mg respectively (table.5.).

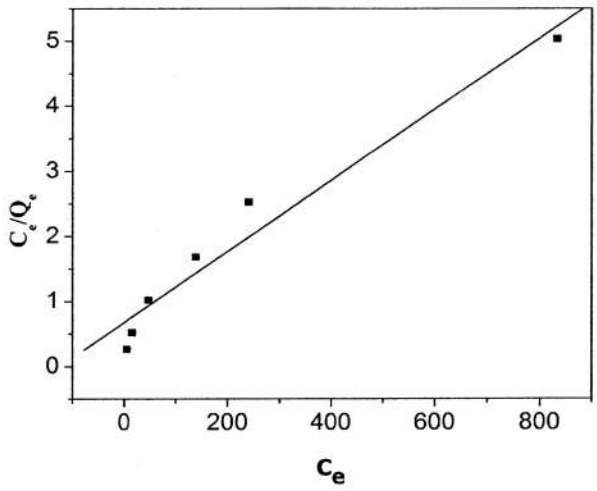

Fig. 23. Langmuir isotherm for adsorption As(V) on CTN

The linear form of Freundlich adsorption equation is represented by the equation

$$\ln Q_e = \ln k_f + \frac{1}{n} \ln C_e \qquad (4)$$

where, Q_e is the adsorbed amount (mg/g), C_e is the equilibrium arsenic concentration (mg/L), K_f (mg/g) is the Freundlich constant related to adsorption capacity and n is constant related to energy of intensity of adsorption. A linear plot of lnQ_e vs $\ln C_e$ is drawn (Fig.24). From the slope and the intercept of the graph, the adsorption capacity, Freundlich constant were obtained and R^2 value which showed the fitting of the data obtained with the isotherm.

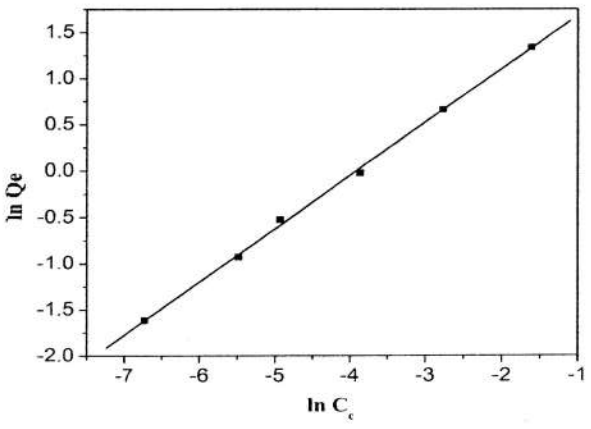

Fig. 24. Freundlich isotherm for the adsorption of As(V) on CTN

Table.5. shows the Langmuir and Freundlich isotherm parameters obtained at room temperature. It was observed that the R^2 values for both Langmuir and Freundlich isotherms showed good co-relations of the data. Thus the sorption could be reasonably explained with both the isotherms. Freundlich isotherm showed better fitting (R^2=1) as compared to Langmuir (R^2=0.947). Moreover the value of n=1.977 (1<n<10, indicates good fitting) also described better fitting of Freundlich isotherm compared to Langmuir model. These informations implied a multilayer physisorption pattern of As(V) on adsorbent surface.

Table. 5. A comparisons of Langmuir and Freundlich isotherm parameters obtained at room temperature

Langmuir parameters				Freundlcih parameters			
Q_0(mg/g)	b (l/mg)	R^2	S. D.	N	k_f(mg.g)	R^2	S .D.
1.48	123.75	0.947	0.202	1.977	9.497	1	0.046

CONCLUSIONS

Composite of clay with chitosan biopolymer was successfully prepared and well employed in As(V) removal. Different characterization techniques confirmed the formation of the composite. XRD and TEM data showed good exfoliation of the clay layers within the polymer matrix. Incorporation of clay in to the system showed prominent improvement in As(V) removal compared to the system without clay. pH is a significant factor for the adsorption process. The sorption was observed to be dependent on material dose, contact time and initial arsenic concentration also. The chitosan-clay system has best efficiency at acidic pH(~3). Both the systems showed a multilayer physisorption pattern as depicted by equilibrium adsorption data. This indicates a good prospect for the desorption step. From the kinetic data, it was observed that although with increase in initial ion concentration percent removal decreasedbut the qe value increased. The sorption in this case was governed by a second order kinetic mechanism.MO seed powder has great potential for removing contaminants from water. But the major disadvantage faced by the use of MO seed was the presence of low molecular

weight water soluble proteins which poses difficulties to separate it from treated water. Incorporation of chitosan biopolymer along with crosslinking agents (glutaraldehyde) improves the stabilisation of MO seed powder. This new system exihibited results which were comparable to those of MO seed. MO and polymer coated MO were not thoroughly studied for removal of As because of the presence of some soluble proteins. The dose of the treated materials (MO, CSMO), treatment time and pH were optimized for fluoride removal. Both MO and polymer coated MO were capable of removing fluoride up to 35% under both acidic and alkaline condition. But still an in depth study is required in order to fully exploit the potential of MO.

The chitosan-iron system was also characterized by FT-IR, XRD, SEM, EDX etc. It showed good magnetic property. The results of this system were similar to the chitosan-clay system. This system had great efficiency for removing arsenic from contaminated water. It can bring down the arsenic level to below 10 ppb i.e. the WHO standard for drinking water. For an initial As(V) concentration of 0.6 mg/L and at neutral pH, a dose of 1.0g/L of CTN was sufficient to bring down the As(V) concentration below 0.01mg/L in 120 min and neutral pH. The sorption and kinetic patterns were similar to the chitosan-clay system.

Manuscripts prepared and Papers presented in Conference during the reported period of the project:

1. Pankaj Gogoi, Ashim J Thakur, S. Banerjee, Rashmi Rekha Devi, Vijay Veer, Boddhaditya Das, Tarun K Maji, Adsorption of As(V) From Contaminated Water on to Chitosan Magnetite Nanoparticle: Equilibrium and kinetics study (*Communicated*).
2. Pankaj Gogoi, Ashim J Thakur, S. Banerjee, Rashmi Rekha Devi, Vijay Veer, Chitosan based nanoparticle for the removal of contaminants from water, (*manuscript under preparation*).
3. Poster presented on "Chitosan Based Nanoparticle for the Removal of Contaminants from Water" in the national conference "Recent Development in Health, Hygiene and Environment" organized by defence research laboratory, Tezpur, Assam, from 6-8th November, 2013.
4. Poster presented on "*Moringa oleifera* Seeds and Its Composite With Chitosan;

Promising Materials for Defluoridation of Water" in the national conference "Recent Advances in Chemical Research" organized by Dept. of Chemistry, Rajib Gandhi University, Arunachal Pradesh, on March 20-21, 2014.

5. Poster presented on "Adsorption of As(V) From Contaminated Water on to Chitosan Magnetite Nanocomposite: Equilibrium Study" organized by North East Hill University, Shillong, on March 3-5, 2015.

FUND UTILIZATION CERTIFICATE

(From July 21' 2011 to Jan' 2015)

1. Title of the project : Development of Bio Nano Composite for Removal of Contaminants from water.

2. Name of Institution : Tezpur University

3. Sanctioned Authority : Defence Research Laboratory

4. Total amount received : Rs. Nine lacs fifty seven thousands two hundred twenty only (Rupees 9,57,220 only)

5. Interest earned : Rs. Seventeen thousand four hundred twelve only (Rupees 17,412 only)

6. Actual expenditure incurred: Rs. Nine lacs eleven thousands five hundred seventy seven only (Rupees 9,11,577 only)

7. Unutilized amount (if any) : Rs. Sixty three thousand fifty five only (Rupees 63,055 only)

8. Already refunded vide : Rs. Forty five thousand six hundred forty three (Rupees 45,643 only) vide D/D no.- "135336"

9. Refundable amount : Rs. Seventeen thousand four hundred twelve (Rupees 17,412 only) vide D/D no.- "569545"

Certified that the terms and conditions, on which the grant-in-aid was sanctioned, have been duly fulfilled and the money was actually utilized for the purpose for which it was sanctioned.

Signature of Chief Financial Authority
Name: D.K . Bhattacharyya
Designation: Finance Officer
Seal: Finance Officer Tezpur University

Signature of PI
Name: T. K. Maji
Designation: Professor
Seal: TARUN K. ... Professor Dept. of Chemical Sciences Tezpur University